


Communication

# Collapse Dynamics of Vortex Beams in a Kerr Medium with Refractive Index Modulation and PT-Symmetric Lattices

Gang Yao, Yuhua Li and Rui-Pin Chen \* 

Key Laboratory of Optical Field Manipulation of Zhejiang Province, Department of Physics, Zhejiang Sci-Tech University, Hangzhou 310018, China; 201920109021@mails.zstu.edu.cn (G.Y.); yuhuali@zstu.edu.cn (Y.L.)

\* Correspondence: chenrp@zstu.edu.cn

**Abstract:** Using the two-dimensional nonlinear Schrödinger equation, the collapse dynamics of vortex beams in a Kerr medium with refractive index modulation and parity–time (PT) symmetric lattices are explored. The critical power for the collapse of vortex beams in a Kerr medium with real optical lattices (i.e., refractive index modulation lattices) was obtained and discussed. Numerical calculations showed that the number of self-focusing points, the locations of the collapse, and the propagation distances for collapse are sensitively dependent on the modulation factors, topological charge numbers, and initial powers. When the vortex optical field propagates in a Kerr medium with real optical lattices, the optical field will collapse into a symmetrical shape. However, the shape of the vortex beam will be chaotically distorted and collapse in asymmetric patterns during propagation in a Kerr medium with PT-symmetric lattices because of the presence of the complex refraction index. Introducing PT-symmetric lattices into nonlinear Kerr materials may offer a new approach to controlling the collapse of vortex beams.

**Keywords:** Kerr nonlinear medium; parity–time symmetry; vortex beam; collapse



**Citation:** Yao, G.; Li, Y.; Chen, R.-P. Collapse Dynamics of Vortex Beams in a Kerr Medium with Refractive Index Modulation and PT-Symmetric Lattices. *Photonics* **2022**, *9*, 249. <https://doi.org/10.3390/photonics9040249>

Received: 9 March 2022

Accepted: 7 April 2022

Published: 10 April 2022

**Publisher's Note:** MDPI stays neutral with regard to jurisdictional claims in published maps and institutional affiliations.



**Copyright:** © 2022 by the authors. Licensee MDPI, Basel, Switzerland. This article is an open access article distributed under the terms and conditions of the Creative Commons Attribution (CC BY) license (<https://creativecommons.org/licenses/by/4.0/>).

## 1. Introduction

The concept of parity–time (PT) symmetry originates from quantum mechanics [1–3], and the potential function should satisfy parity  $V(x, y) = V^*(-x, -y)$  with \* standing for complex conjugate in a PT-symmetric system. In optics region, the wave equation is similar in mathematical form to the Schrödinger equation under the quantum mechanism. Since the PT-symmetric potential can be achieved by the complex refractive index (the real part is the refractive index, while the imaginary part determines gain–loss) distribution  $n(x, y) = n_R(x, y) + in_I(x, y)$  in an optical material system, it has been successfully introduced into the optics region [3,4]. The refractive indices of the real and imaginary parts are required to satisfy the even and odd function, i.e.,  $n(x, y) = n^*(-x, -y)$ . Many new physical phenomena have been observed in this special structure and have been widely used in various branches of physics [5–7]. Especially, it has been discussed extensively in the field of the nonlinear PT-symmetric system such as the existence and stability of soliton, the solitons control, and the evolution and polarization properties of vector vortex beams in the nonlinear medium with PT-symmetric optical lattices [8–11].

The collapse and filaments of an optical field in nonlinear materials are especially interesting due to the fact of this special physical property and have been intensively studied experimentally and theoretically in recent years [12–14]. When an optical field with an initial power higher than a certain threshold propagates in a self-focusing medium, the nonlinear collapse of the optical field will occur. If the initial power continues to increase sufficiently, other nonlinear effects will follow such as plasma generation, multiple collapse spots, forming its own filament, and higher-order nonlinearity [15–17]. Due to the many potential applications of this special physical property, the collapse of an optical field and the design of the controllable filaments have been the focus of attention such as on the

control of helical filaments by twisted beams [18], the dynamic collapse of Airy and vortex Airy beam [19], and the ellipticity of the input beam and laser filamentation [20,21].

Vortex with a screw phase dislocation, which results in an orbital angular momentum, has become a hot topic of research because of its fundamental interest and numerous applications such as the fractional vortex beam [22], the optical angular momentum [23–25], optical field manipulation [26,27], optical tweezer [28,29], quantum information processing [30], and special vortex beams with open rings [31]. In particular, the interaction of vortex beams with a nonlinear material has led to many novel phenomena [32]. Kruglov et al. derived theoretically the critical powers of vortex in a Kerr nonlinear material [33]. Fibich et al. numerically calculated the actual critical powers of vortices in the Kerr medium [34]. Vortex beams with spatially inhomogeneous polarization distributions have provided new insights into collapse properties of optical fields [12,35]. Recently, the evolution of vector vortex optical fields in strongly nonlocal nonlinear media with PT-symmetric potential has been theoretically demonstrated [11]. The vector vortex optical field propagates reciprocally in cycles in such optical materials despite the existence of a PT-symmetric optical lattice, and there is a conversion between the linear and circular polarization states during propagation. In this work, the collapse dynamics of vortex optical fields in nonlinear Kerr media with PT-symmetric lattices were explored. The effect of Kerr nonlinearity (self-focusing effect) resulted in the nonlinear collapse of the vortex optical field, and the periodic evolution phenomenon could not occur. The critical power required to keep the root mean square beam width invariant for the vortex optical field collapse in a Kerr medium with real optical lattices (i.e., refractive index modulation lattices) was theoretically derived based on the nonlinear Schrödinger equation [36]. Numerical calculations suggest that the number of self-focusing points, the locations of the collapse, and the propagation distances for collapse are sensitively dependent on the modulation factors, topological charge numbers, and initial powers. When the vortex optical field propagates in the Kerr medium with real optical lattices, the optical field will collapse into a symmetrical shape due to the effect of refractive index modulation lattices. On the other hand, the vortex beam will be chaotically distorted and collapse into asymmetrical patterns due to the modulation of complex refraction index during propagation in the Kerr medium with PT-symmetric lattices. These results provide a deeper understanding of the manipulation and fundamental dynamics of the nonlinear collapse of a vortex beam.

## 2. Theoretical Model

Under the paraxial approximation condition, the evolution of vortex optical fields in the nonlinear Kerr medium with PT-symmetric potentials is governed through the dimensionless two-dimensional nonlinear Schrödinger equation [16]:

$$\nabla_{\perp}^2 E + i \frac{\partial E}{\partial \zeta} + R(\eta, \zeta)E + |E|^2 E = 0 \tag{1}$$

where  $\nabla_{\perp}^2$ , in the first term of Equation (1), represents the two-dimensional Laplace operator. Here,  $\eta = x/w_0$  and  $\zeta = y/w_0$  are the dimensionless transverse, where  $w_0$  is the beam width.  $\zeta = z/(2kw_0^2)$  are the longitudinal coordinates representing the direction of beam propagation, where  $k$  is the wave number. For PT-symmetric optical lattices (complex refractive index structure), the real and imaginary parts are, respectively, denoted by  $V(\eta, \zeta)$  and  $W(\eta, \zeta)$ , satisfying  $R(\eta, \zeta) = V_0 V(\eta, \zeta) + iW_0 W(\eta, \zeta)$  [3]. The real and imaginary parts, respectively, represent refractive index and gain–loss in optics;  $V_0$  and  $W_0$  are their modulation depths. We considered the SCPT that had the following form [4]:

$$\begin{aligned} V(\eta, \zeta) &= \cos^2(\eta/d) + \cos^2(\zeta/d), \\ W(\eta, \zeta) &= \sin(2\eta/d) + \sin(2\zeta/d) \end{aligned} \tag{2}$$

Here,  $d$  denotes modulation factors of complex refractive index that controls the PT-symmetric lattice density. The specific complex refractive index distribution can be achieved by adjusting various parameters in the  $R(\eta, \zeta)$  function.

A typical vortex beam is used as the initial field:

$$E(\eta, \zeta, \xi = 0) = A_0 \rho^n \exp(-\rho^2) e^{in\varphi} \tag{3}$$

where  $A_0$  is a constant;  $n$  is the topological charge number of vortex beams;  $\rho = \sqrt{\eta^2 + \zeta^2}$  and  $\varphi$  represent the polar radius and azimuthal angle, respectively. Figure 1a is a stereoscopic view of the interaction of vortex beams with Kerr-SCPT media. When  $d$  was 0.23 and 0.31, the complex refractive index (Kerr-SCPT medium) distributions are shown in Figure 1b,c, respectively. Furthermore, the modulation without gain-loss in the medium is for the case of  $V_0 \neq 0$  and  $W_0 = 0$ , which is a Kerr medium with real optical lattice potential (Kerr-ROLP medium).

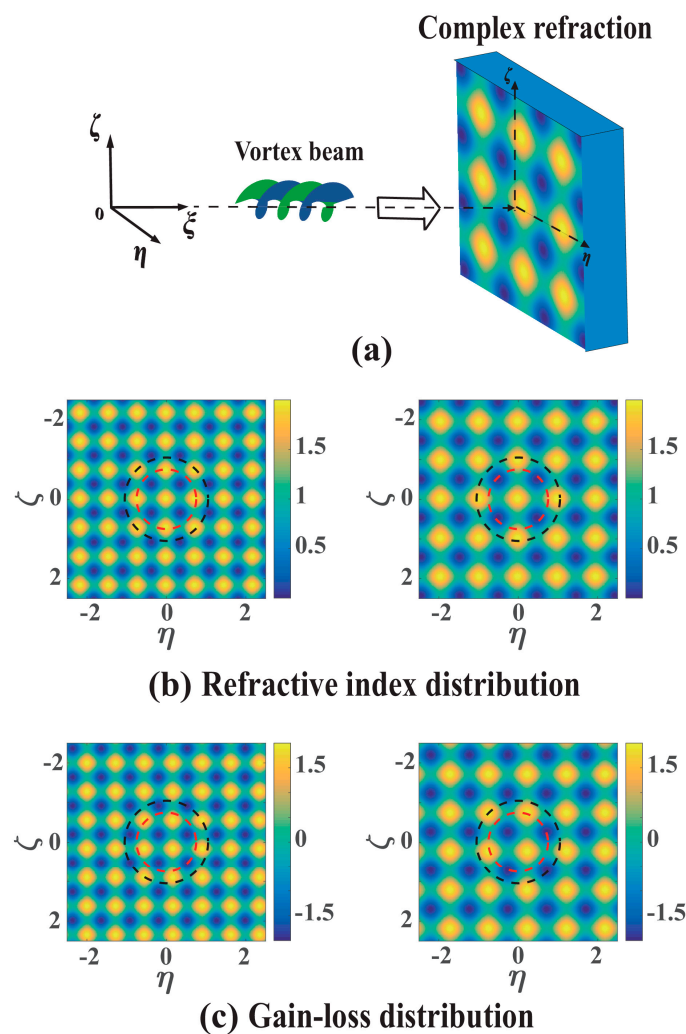


**Figure 1.** Diagrammatic sketch of vortex beams in a Kerr-SCPT medium: (a) the interaction between vortex beams and the Kerr-SCPT medium; (b) refractive index distribution, the left plot  $d = 0.23$ , the right plot  $d = 0.31$ ; (c) gain-loss distribution, the left plot  $d = 0.23$ , the right plot  $d = 0.31$ . The black and the red dashed ring lines overlapped in (c) represent the initial beam width when the vortex topological charge was  $n = 1$  and  $n = 2$ , respectively.

There are several important quantities of the nonlinear Schrödinger equation: the initial power  $P(\xi) = \int \int_s |E|^2 d\eta d\zeta$ , the Hamiltonian  $H(\xi) = \int \int_s (|\nabla E|^2 - V_0(\cos^2(\eta/d) + \cos^2(\zeta/d))|E|^2 - 1/2|E|^4) d\eta d\zeta$ , and the root mean square beam width defined as  $W(\xi) = \int \int_s (\eta^2 + \zeta^2) |E|^2 d\eta d\zeta$ . When  $H(\xi) = 0$  and  $W_0 = 0$ , which means that there is a total balance between the propagation diffraction effect and the self-focusing effect in the Kerr-ROLP medium [19,37], then, the amplitude  $A_0$  can be obtained by substituting the expression  $E(\eta, \zeta, \xi = 0)$  of the vortex optical field into  $H(\xi = 0) = 0$ . Thus, the critical power ( $P_{cr}$ ) in the Kerr-ROLP medium required for the collapse of a vortex optical field can be obtained as:

$$P_{cr} = \frac{2^{2n+2}\pi\Gamma(n+1)\Gamma(n+2)}{\Gamma(2n+1)} - \frac{2^{2n}V_0\Gamma(n+1)}{\Gamma(2n+1)} \cdot G(n) \tag{4}$$

where  $G(n) = \sum_{k=0}^n \binom{n}{k} \Gamma(k + \frac{1}{2})\Gamma(n - k + \frac{1}{2}) ({}_1F_1(n - k + \frac{1}{2}; \frac{1}{2}; -\frac{1}{2d^2}) + {}_1F_1(k + \frac{1}{2}; \frac{1}{2}; -\frac{1}{2d^2}) + 2)$  with the Gamma function,  $\Gamma(\cdot)$ , and the hypergeometric function,  ${}_1F_1(\alpha, \beta, z)$ . Obviously, the modulation depth ( $V_0$ ), the vortex topological charge number ( $n$ ), and the modulation factor ( $d$ ) determine the value of  $P_{cr}$ . By setting  $V_0 = 0$  in Equation (4),  $P_{cr} = 4^n\Gamma(n+1)\Gamma(n+2)/\Gamma(2n+1) P_G$  represents the critical power of a vortex optical field in the Kerr medium, where  $P_G$  denotes the critical power of a Gaussian beam, as given in [33]. Due to the impact of the refractive index contribution of the Kerr-ROLP medium, the critical power ( $P_{cr}$ ) of vortex beams in a Kerr-ROLP medium is lower than that in a Kerr medium. The critical power of vortex beams in the Kerr-ROLP medium indicates a total compromise of the competition among the propagation diffraction effect, the periodic lattice refraction index modulation and the nonlinear self-focusing effect. When the input power  $P_{in} = P_{cr}$ , the root-mean square beam width remains invariant. As input powers exceed the threshold  $P_{cr}$ , the beam evolves into a global collapse, and the beam width is reduced to 0 within a limited distance [38]. However, the critical power mentioned here is the upper limit of the vortex beam collapse in practice, and the actual partial collapse has occurred before the input power ( $P_{in}$ ) approaches the critical power ( $P_{cr}$ ) for cases where incident beams are not the Townes profile [38,39].

### 3. Numerical Simulation and Analysis

Numerical results were obtained to further study the collapse dynamics of the vortex beam with  $w_0 = 10$  and  $\lambda = 0.53 \mu\text{m}$  in the Kerr-SCPT medium, based on the split-step finite difference method [37].

For a Kerr-ROLP medium ( $V_0 \neq 0, W_0 = 0$ ) with symmetry distributions of refractive index with different modulation factors and modulation depths, the evolution of the intensity distributions in the cross-section of the vortex beam with the different vortex topological charge numbers,  $n = 1$  and  $2$ , are shown in Figure 2a,b, respectively. As the propagation distance increased, the ring-shaped vortex beams with different radii gradually split into several focus points within certain propagation distances as shown in Figure 2. For the case of  $n = 1$ , four focus points were found at the periphery ring of the vortex beam and finally collapsed into four points when  $d = 0.23$  and  $0.31$ , respectively, as shown in the upper two rows of Figure 2a. For the case of  $n = 2$ , the beam was initially split into eight focal points with different intensities and finally collapsed into four collapse points as shown in Figure 2b. As well known, the beams will perform self-focusing behavior during propagation in a nonlinear Kerr medium. However, the energy cannot be accumulated in the vortex beam center, since there is an optical singularity in the center of the vortex optical field; thus, the vortex optical field will autofocus into a light ring. Eventually, the optical field evolves into even number of foci due to the modulation of the optical lattices as shown in Figure 2. The number of the partial collapses depends on the initial powers [15–17,37], and the number of partial collapses will increase with the increasing initial powers. For the cases of modulation factors  $d = 0.23$  and  $0.31$ , the location of the final beam collapse was different as shown in the upper two rows of Figure 2. The vortex optical field will initially form some focal points, positions of which are greatly influenced by the refractive index

distribution of the real optical lattice (compare Figures 1b and 2). The relative positions of high refractive index in the autofocusing light ring depend on the vortex topological charge number and the modulation factor  $d$ . The positions of the foci in the autofocusing light ring with  $d = 0.23$  and  $n = 1$  are different to that of  $d = 0.23$  and  $n = 2$ , as shown in Figure 2. In particular, due to the existence of the vortex, these focal points and the optical field will rotate during propagation.

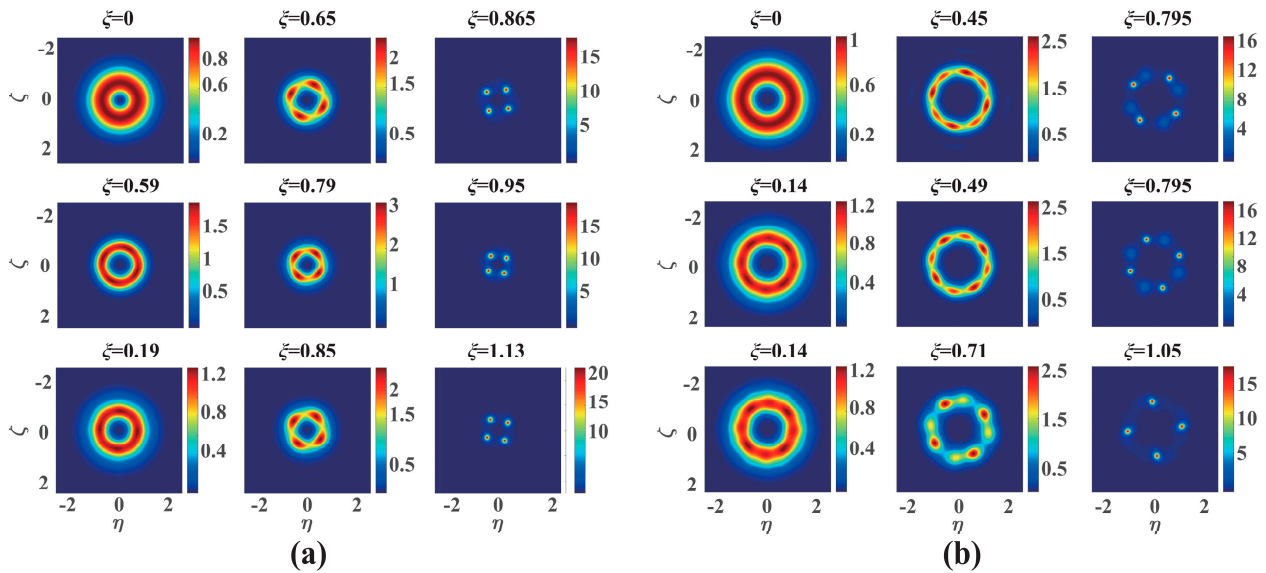


**Figure 2.** The evolution of vortex beams in a Kerr-ROLP medium for different modulation depths and modulation factors. (a)  $n = 1$ ,  $P_{in} = 1.7P_{cr}$ , the first to the third rows are, respectively, with  $V_0 = 0.2$ ,  $d = 0.31$ ;  $V_0 = 0.2$ ,  $d = 0.23$ ;  $V_0 = 0.7$ ,  $d = 0.23$ . (b)  $n = 2$ ,  $P_{in} = 1.4P_{cr}$ , the first to the third rows are, respectively, with  $V_0 = 0.9$ ,  $d = 0.31$ ;  $V_0 = 0.9$ ,  $d = 0.23$ ;  $V_0 = 1.8$ ,  $d = 0.23$ .

The peak intensity of vortex beams is shown in Figure 3, which is a function of the transmission length. It should be noted here that the increase in the value of  $V_0$  will lead to a decrease in the critical power (see Equation (4)). In order to analyze the impact of the modulation depth  $V_0$  on the propagation distance for collapse, the same initial powers should be taken for the comparisons. When  $n = 1$  and  $V_0 = 0.2$ , the initial power  $P_{in} = 1.7P_{cr} = 6.46P_G$ , and if  $n = 1$  and  $V_0 = 0.7$ , then  $P_{in} = 1.7P_{cr} = 5.61P_G$ . For the case  $n = 2$  and  $V_0 = 0.9$ , the initial power  $P_{in} = 1.4P_{cr} = 9.52P_G$ , and if  $n = 2$  and  $V_0 = 1.8$ , the initial  $P_{in} = 1.4P_{cr} = 7.83P_G$ . It can be seen from Figure 3 that the distance required for the beam collapse decreased as  $V_0$  increased. This is because with the increase in the value of  $V_0$ , the modulation effect of the refractive index gradient of the optical lattice was enhanced, leading to the higher optical intensity at the focus point and vice versa. Therefore, the number of focus points, the transmission length of the collapsed vortex beams, and the locations of the collapse were closely related to the refractive index distribution of the optical lattice. In addition, the propagation distances required for collapse decrease with increasing initial powers. When the input power  $P_{in} = 6.46P_G$ , the distance required for the collapse of the vortex beam of  $n = 1$  was shorter than  $\zeta = 1$ , but when  $P_{in} = 5.61P_G$ , the collapse distance was longer than  $\zeta = 1$  (see Figure 3a). Similarly, the collapse distances of the vortex beam with  $P_{in} = 9.52P_G$  were shorter than that of  $P_{in} = 7.83P_G$  if  $n = 2$  (see Figure 3b).



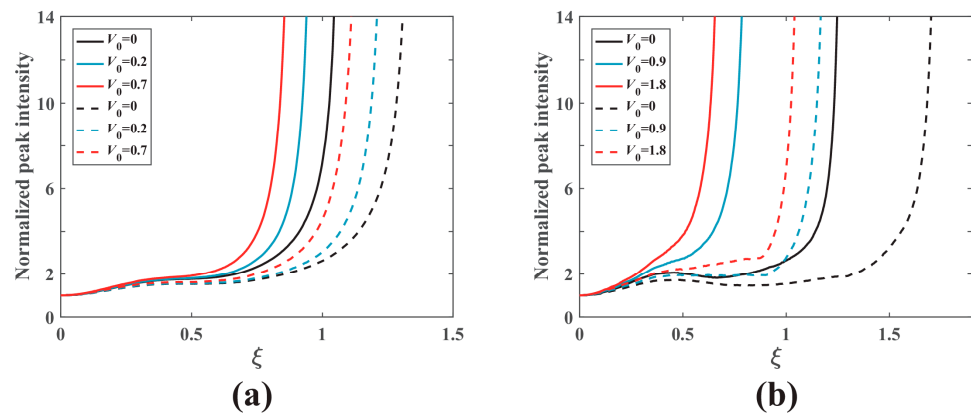


**Figure 3.** The normalized peak intensity of vortex beams with  $d = 0.23$  in a Kerr–ROLP medium for different modulation depths as a function of transmission length. (a)  $n = 1$  with different initial powers:  $P_{in} = 6.46P_G$  (i.e.,  $1.7P_{cr}$  for  $V_0 = 0.2$  (solid lines));  $P_{in} = 5.61P_G$  (i.e.,  $1.7P_{cr}$  for  $V_0 = 0.7$  (dashed lines)). (b)  $n = 2$  with different initial powers:  $P_{in} = 9.52P_G$  (i.e.,  $1.4P_{cr}$  for  $V_0 = 0.9$  (solid lines));  $P_{in} = 7.83P_G$  (i.e.,  $1.4P_{cr}$  for  $V_0 = 1.8$  (dashed lines)).

For the Kerr–SCPT medium ( $V_0 \neq 0, W_0 \neq 0$ ), the gain–loss (complex refractive index) was introduced, which was different from the conventional optical lattice (ROLP) with only refractive index modulation. The collapse evolution of the vortex beam with different modulation depths of gain–loss was further explored in a Kerr–SCPT medium as shown in Figure 4 for  $n = 1$  and  $n = 2$ . The spatial intensity evolution of vortex optical fields with different vortex topological charge numbers in the Kerr–SCPT medium is shown in the first plots in each panel in Figure 4. The evolution of the vortex optical fields in the Kerr–SCPT medium exhibited asymmetry and distortion different from that in a Kerr–ROLP medium. The initial ring-shaped beam with  $V_0 = 1$  and  $d = 0.31$  was also initially split into four and eight focal points for topological charges  $n = 1$  and  $2$ , respectively, but the beam had different intensity distributions at different positions as shown in Figure 4, unlike in the Kerr–ROLP medium where the optical intensity was symmetrically distributed at each focus point as shown in Figure 2. This was because the optical fields were further modulated by the gain–loss part of the PT-symmetric lattices, resulting in a non-uniform and asymmetrical distribution of the optical intensity in the cross-section of the vortex beam. The intensity distributions were sensitively dependent on the gain–loss distribution (see Figures 1c and 4), and the beam eventually collapsed at these high-intensity points. The relative gain–loss positions in the autofocusing light ring depended on the vortex topological charge number and the modulation factor  $d$ . For the same modulation factor  $d = 0.31$ , the positions of the foci in the light ring with  $n = 1$  were different to that of  $n = 2$  as shown in Figure 4.

The normalized peak intensity is shown in Figure 5, which is a function of the transmission length of vortex beams for different gain–loss modulation depths  $W_0$  for  $n = 1$  and  $n = 2$ . The propagation distance required for collapse in the Kerr–SCPT medium was shorter than that in a Kerr–ROLP medium due to the modulation of gain–loss. The propagation distances required for collapse decreased with the increasing gain–loss modulation  $W_0$ , as shown in Figure 5. The number of focus points, the distance required to collapse, and the location of the collapse were closely related to the topological charge number of the vortex beam, complex refractive index distribution, and input power. Therefore, the special collapse modes and the locations of the collapse can be manipulated by purposely choosing the vortex topological charges, complex refractive index distributions in nonlinear media, and the input powers.

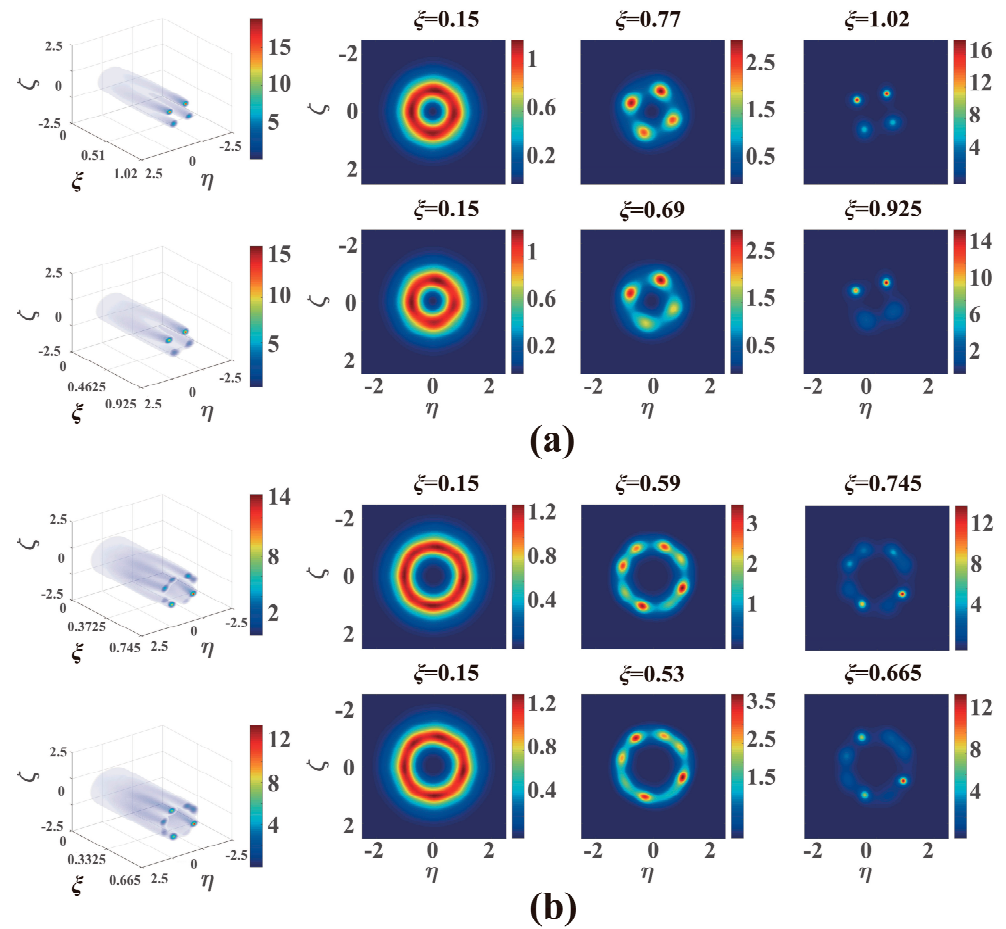


**Figure 4.** The evolution of vortex optical fields in the Kerr-SCPT medium with different modulation depths of gain-loss  $W_0$ . Here,  $V_0 = 1, d = 0.31$ : (a)  $n = 1, P_{in} = 1.7P_{cr}$  with  $W_0 = 0.15$  (upper row) and  $W_0 = 0.45$  (lower row). (b)  $n = 2, P_{in} = 1.4P_{cr}$  with  $W_0 = 0.15$  (upper row) and  $W_0 = 0.45$  (lower row). The spatial evolutions of the vortex beams in the Kerr-SCPT medium are shown in the first plots in each panel.

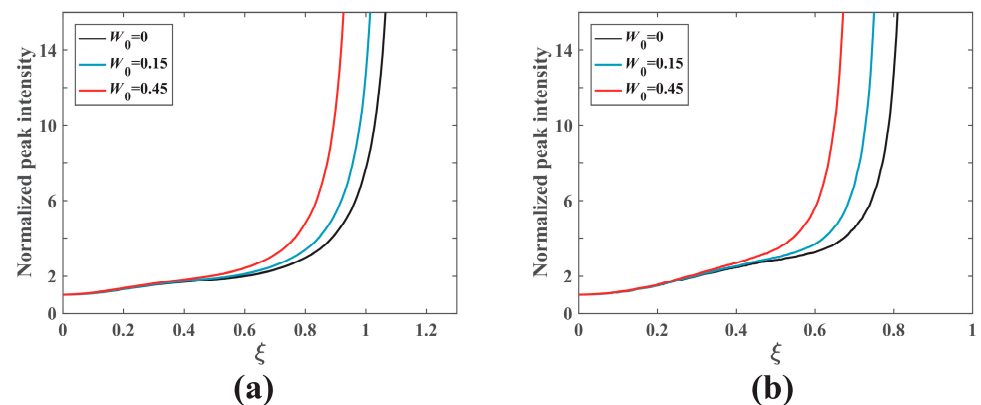


**Figure 5.** The normalized peak intensity of vortex beams with  $V_0 = 1$  and  $P_{in} = 1.4P_{cr}$  as a function of the propagation distance for different modulation depths of gain-loss  $W_0$  in the Kerr-SCPT and Kerr-ROLP media ( $W_0 = 0$ ). The plots (a) and (b) correspond to  $n = 1$  and  $2$ , respectively.

#### 4. Discussion

The nonlinear collapse and filament of the optical field are critical in nonlinear optics due to the fundamental physics and potential applications. The control and manipulation of the collapse of an optical field are a challenging topic. In particular, the collapse behavior of vortex optical fields has received extensive attention such as collapse of vortex Airy beams [37], the generation of plasma filaments to guide microwave radiation [40], and laser filament of complex vector vortex optical fields [41]. However, the collapse dynamics of a vortex optical field in the Kerr medium with PT-symmetric potentials was more likely to extend our understanding of the fundamental collapse dynamics of a vortex beam and can provide the possibility to manipulate the collapse of a vortex optical field. In this work, the collapse dynamics of vortex optical fields in Kerr media with refractive index modulation and PT-symmetric lattices were theoretically demonstrated. In a Kerr medium with a refractive index modulation optical lattice (without gain–loss), the vortex beam initially formed focal points with a symmetrical distribution of the optical intensity. The optical field eventually collapsed into a symmetrical shape due to the self-focusing effect, the propagation diffraction effect, and the periodic lattice refraction index modulation. On the other hand, when in a Kerr medium with PT-symmetric lattices (include gain–loss modulation), the vortex beam will be chaotically distorted during propagation due to the modulation of complex refraction index, and partial collapse occurs in an asymmetrical pattern. Therefore, these results provide the possibility to manipulate the collapse of the vortex beam by adjusting the distribution of the complex refractive index (the modulation factor).

#### 5. Conclusions

Using the two-dimensional nonlinear Schrödinger equation, the collapse dynamics of vortex beams in a Kerr medium with real optical lattices and PT-symmetric potentials were explored. The critical power for the collapse of vortex beams in a Kerr–ROLP medium was theoretically derived and discussed. Numerical results derived by using the split-step finite difference method indicate that the number of focal points, the locations of the collapse, and the propagation distance for collapse in a Kerr–ROLP medium are dependent on the intensity distribution of the refractive index distributions, initial powers, and vortex topological charge numbers. The vortex optical field will collapse in a symmetrical shape when it propagates in a Kerr medium with real optical lattices. On the other hand, the vortex beam became distorted during evolution in a Kerr–SCPT medium due to the existence of the gain–loss; meanwhile, the propagation distances for collapse were shorter than that in a Kerr–ROLP medium. In addition, the beam rotated about the propagation direction during the evolution due to the existence of vortex.

**Author Contributions:** Conceptualization, R.-P.C.; methodology, R.-P.C.; validation, R.-P.C. and Y.L.; investigation, G.Y. and R.-P.C.; data curation, G.Y., R.-P.C. and Y.L.; supervision, R.-P.C.; writing—original draft preparation, G.Y.; writing—review and editing, R.-P.C. and Y.L. All authors have read and agreed to the published version of the manuscript.

**Funding:** This research was funded by the Zhejiang Provincial Key Research and Development Program (grant no. 2022C04007) and the National Natural Science Foundation of China (grant nos. 11874323 and 62105291).

**Institutional Review Board Statement:** Not applicable.

**Informed Consent Statement:** Not applicable.

**Data Availability Statement:** Not applicable.

**Conflicts of Interest:** The authors declare no conflict of interest.



## References

1. Bender, C.M.; Boettcher, S. Real spectra in non-Hermitian Hamiltonians having PT symmetry. *Phys. Rev. Lett.* **1998**, *80*, 5243. [[CrossRef](#)]
2. Bender, C.M.; Dunne, G.V.; Meisinger, P.N. Complex periodic potentials with real band spectra. *Phys. Lett. A* **1999**, *252*, 272–276. [[CrossRef](#)]
3. El-Ganainy, R.; Makris, K.; Christodoulides, D.; Musslimani, Z.H. Theory of coupled optical PT-symmetric structures. *Opt. Lett.* **2007**, *32*, 2632–2634. [[CrossRef](#)] [[PubMed](#)]
4. Makris, K.G.; El-Ganainy, R.; Christodoulides, D.; Musslimani, Z.H. Beam dynamics in PT symmetric optical lattices. *Phys. Rev. Lett.* **2008**, *100*, 103904. [[CrossRef](#)] [[PubMed](#)]
5. Klaiman, S.; Günther, U.; Moiseyev, N. Visualization of branch points in PT-symmetric waveguides. *Phys. Rev. Lett.* **2008**, *101*, 80402. [[CrossRef](#)] [[PubMed](#)]
6. Schwarz, L.; Cartarius, H.; Musslimani, Z.H.; Main, J.; Wunner, G. Vortices in Bose-Einstein condensates with PT-symmetric gain and loss. *Phys. Rev. A* **2017**, *95*, 53613. [[CrossRef](#)]
7. Zhu, X.; Yang, F.; Cao, S.; Xie, J.; He, Y. Multipole gap solitons in fractional Schrödinger equation with parity-time-symmetric optical lattices. *Opt. Express* **2020**, *28*, 1631–1639. [[CrossRef](#)]
8. Hu, S.; Ma, X.; Lu, D.; Yang, Z.; Zheng, Y.; Hu, W. Solitons supported by complex PT-symmetric Gaussian potentials. *Phys. Rev. A* **2011**, *84*, 43818. [[CrossRef](#)]
9. Fan, Z.; Malomed, B.A. Dynamical control of solitons in a parity-time-symmetric coupler by periodic management. *Commun. Nonlinear Sci. Numer. Simul.* **2019**, *79*, 104906. [[CrossRef](#)]
10. Chen, Y.; Yan, Z.; Mihalache, D. Soliton formation and stability under the interplay between parity-time-symmetric generalized Scarf-II potentials and Kerr nonlinearity. *Phys. Rev. E* **2020**, *102*, 12216. [[CrossRef](#)] [[PubMed](#)]
11. Yao, G.; Chew, K.H.; Wu, Y.; Li, Y.; Chen, R.P. Propagation dynamics of vector vortex beams in a strongly nonlocal nonlinear medium with parity-time-symmetric potentials. *J. Opt.* **2022**, *24*, 35606. [[CrossRef](#)]
12. Chen, R.P.; Chew, K.H.; Zhou, G.; Dai, C.Q.; He, S. Vectorial effect of hybrid polarization states on the collapse dynamics of a structured optical field. *Opt. Express* **2016**, *24*, 28143–28153. [[CrossRef](#)] [[PubMed](#)]
13. Lan, J.; Yu, C.; Liu, Y.; Feng, Z.; Fu, L.; Liu, J. Effects of delayed Kerr nonlinearity on the propagation of femtosecond annular Gaussian filaments in air. *Phys. Scr.* **2019**, *94*, 105225. [[CrossRef](#)]
14. Thul, D.; Richardson, M.; Rostami Fairchild, S. Spatially resolved filament wavefront dynamics. *Sci. Rep.* **2020**, *10*, 8920. [[CrossRef](#)] [[PubMed](#)]
15. Bergé, L. Wave collapse in physics: Principles and applications to light and plasma waves. *Phys. Rep.* **1998**, *303*, 259–370. [[CrossRef](#)]
16. Bergé, L.; Gouédard, C.; Schjødt-Eriksen, J.; Ward, H. Filamentation patterns in Kerr media vs. beam shape robustness, nonlinear saturation and polarization states. *Phys. D* **2003**, *176*, 181–211. [[CrossRef](#)]
17. Kolesik, M.; Wright, E.; Moloney, J. Femtosecond filamentation in air and higher-order nonlinearities. *Opt. Lett.* **2010**, *35*, 2550–2552. [[CrossRef](#)]
18. Lü, J.Q.; Li, P.P.; Wang, D.; Tu, C.; Li, Y.; Wang, H.T. Control on helical filaments by twisted beams in a nonlinear CS<sub>2</sub> medium. *Opt. Express* **2018**, *26*, 29527–29538. [[CrossRef](#)] [[PubMed](#)]
19. Chen, R.P.; Yin, C.F.; Chu, X.X.; Wang, H. Effect of Kerr nonlinearity on an Airy beam. *Phys. Rev. A* **2010**, *82*, 43832. [[CrossRef](#)]
20. Dubietis, A.; Tamosauskas, G.; Fibich, G.; Ilan, B. Multiple filamentation induced by input-beam ellipticity. *Opt. Lett.* **2004**, *29*, 1126–1128. [[CrossRef](#)]
21. Jin, Z.; Zhang, J.; Xu, M.; Lu, X.; Li, Y.; Wang, Z.; Wei, Z.; Yuan, X.; Yu, W. Control of filamentation induced by femtosecond laser pulses propagating in air. *Opt. Express* **2005**, *13*, 10424–10430. [[CrossRef](#)] [[PubMed](#)]
22. Zhang, H.; Zeng, J.; Lu, X.; Wang, Z.; Zhao, C.; Cai, Y. Review on fractional vortex beam. *Nanophotonics* **2022**, *11*, 241–273. [[CrossRef](#)]
23. Berkhout, G.C.; Lavery, M.P.; Courtial, J.; Beijersbergen, M.W.; Padgett, M.J. Efficient sorting of orbital angular momentum states of light. *Phys. Rev. Lett.* **2010**, *105*, 153601. [[CrossRef](#)] [[PubMed](#)]
24. Yang, Y.; Zhao, Q.; Liu, L.; Liu, Y.; Rosales-Guzmán, C.; Qiu, C.W. Manipulation of orbital-angular-momentum spectrum using pinhole plates. *Phys. Rev. Appl.* **2019**, *12*, 64007. [[CrossRef](#)]
25. Bai, Y.; Lv, H.; Fu, X.; Yang, Y. Vortex beam: Generation and detection of orbital angular momentum. *Chin. Opt. Lett.* **2022**, *20*, 12601. [[CrossRef](#)]
26. Dholakia, K.; Čižmár, T. Shaping the future of manipulation. *Nat. Photonics* **2011**, *5*, 335–342. [[CrossRef](#)]
27. Yang, Y.; Ren, Y.; Chen, M.; Arita, Y.; Rosales-Guzmán, C. Optical trapping with structured light: A review. *Adv. Photonics* **2021**, *3*, 34001. [[CrossRef](#)]
28. Padgett, M.; Bowman, R. Tweezers with a twist. *Nat. Photonics* **2011**, *5*, 343–348. [[CrossRef](#)]
29. Paterson, L.; MacDonald, M.P.; Arlt, J.; Sibbett, W.; Bryant, P.; Dholakia, K. Controlled rotation of optically trapped microscopic particles. *Science* **2001**, *292*, 912–914. [[CrossRef](#)]
30. Li, Z.X.; Ruan, Y.P.; Chen, P.; Tang, J.; Hu, W.; Xia, K.Y.; Lu, Y.Q. Liquid crystal devices for vector vortex beams manipulation and quantum information applications. *Chin. Opt. Lett.* **2021**, *19*, 112601. [[CrossRef](#)]

31. Zeng, R.; Zhao, Q.; Shen, Y.; Liu, Y.; Yang, Y. Structural stability of open vortex beams. *Appl. Phys. Lett.* **2021**, *119*, 171105. [[CrossRef](#)]
32. Song, L.; Yang, Z.; Zhang, S.; Li, X. Spiraling anomalous vortex beam arrays in strongly nonlocal nonlinear media. *Phys. Rev. A* **2019**, *99*, 63817. [[CrossRef](#)]
33. Kruglov, V.; Logvin, Y.A.; Volkov, V. The theory of spiral laser beams in nonlinear media. *J. Mod. Opt.* **1992**, *39*, 2277–2291. [[CrossRef](#)]
34. Fibich, G.; Gavish, N. Critical power of collapsing vortices. *Phys. Rev. A* **2008**, *77*, 45803. [[CrossRef](#)]
35. Chen, R.P.; Zhong, L.X.; Chew, K.H.; Zhao, T.Y.; Zhang, X. Collapse dynamics of a vector vortex optical field with inhomogeneous states of polarization. *Laser Phys.* **2015**, *25*, 75401. [[CrossRef](#)]
36. Perez-Garcia, V.M.; Torres, P.J.; Montesinos, G.D. The method of moments for nonlinear Schrödinger equations: Theory and applications. *SIAM J. Appl. Math.* **2007**, *67*, 990–1015. [[CrossRef](#)]
37. Chen, R.P.; Chew, K.H.; He, S. Dynamic control of collapse in a vortex Airy beam. *Sci. Rep.* **2013**, *3*, 1406. [[CrossRef](#)] [[PubMed](#)]
38. Fibich, G.; Gaeta, A.L. Critical power for self-focusing in bulk media and in hollow waveguides. *Opt. Lett.* **2000**, *25*, 335–337. [[CrossRef](#)]
39. Chiao, R.Y.; Garmire, E.; Townes, C.H. Self-trapping of optical beams. *Phys. Rev. Lett.* **1964**, *13*, 479. [[CrossRef](#)]
40. Polynkin, P.; Ament, C.; Moloney, J.V. Self-focusing of ultraintense femtosecond optical vortices in air. *Phys. Rev. Lett.* **2013**, *111*, 23901. [[CrossRef](#)]
41. Meyer, H.J.; Mamani, S.; Alfano, R.R. Steady-state stimulated Raman generation and filamentation using complex vector vortex beams. *Appl. Opt.* **2020**, *59*, 6245–6251. [[CrossRef](#)] [[PubMed](#)]